

Electronic Supplementary Information for

**Hyperactive iron carbide@N-doped reduced graphene
oxide/carbon nanotube hybrid architecture for a rapid CO
hydrogenation**

Beum Jin Park,^a Sanha Jang,^b Jin Hee Lee,^b Dong Hyun Chun,^b Ji Chan Park,^{,b} Ho Seok
Park^{*,a,c}*

^a School of Chemical Engineering, Sungkyunkwan University, 2066, Seoburo, Jangan-gu,
Suwon 440-746, Republic of Korea

^b Clean Fuel Laboratory, Korea Institute of Energy Research, 152 Gajeong-Ro,
Yuseong-Gu, Daejeon, 34129, Republic of Korea

^c SKKU Advanced Institute of Nano Technology (SAINT), Sungkyunkwan University,
2066, Seoburo, Jangan-gu, Suwon 440-746, Republic of Korea

Experimental Section

Chemicals: Porphyrine (Iron(II) phthalocyanine ($C_{32}H_{16}FeN_8$)), ferrocene ($Fe(C_5H_5)_2$), iron (III) nitrate nonahydrate ($Fe(NO_3)_3 \cdot 9H_2O$), and azodicarboxamide (ADC, $C_2H_4O_2N_4$, 97%) were purchased from Aldrich. Acetonitrile (CH_3CN , 99.8 %) and hypophosphorous acid (H_3PO_2 , 50 wt %) were obtained from Samchun Chemical. Iodine (I_2 , 99.0 %) and activated carbon were purchased from Daejung Co. Ltd and Strem, respectively. All reagents were used as received without further purification.

Steam activation of reduced graphene oxide: Graphene oxide (GO) was prepared by modified Hummers method. GO powder was then dispersed in DI-water by stirring it at 300 rpm. To the GO dispersions, hypophosphorous acid and iodine were mixed. Then mixture was allowed to react at $80^\circ C$ for 12 h. During the time, reduction of GO took place and self-assembled rGO monolith was formed. The gel was then washed by distilled water until pH 7, the gel was then frozen with the help of liquid nitrogen and freeze dried. The steam activation method was used to generate the defects and activate the rGO surface. For activation, the rGO was heated up to $900^\circ C$ in a tube furnace at a heating rate $5^\circ C \cdot min^{-1}$ with N_2 gas. Once the temperature reached to $900^\circ C$, the steam was purged inside at the steam flow rate of $0.167 mL \cdot h^{-1}$ for 1h. Steam activation rGO (s-rGO) obtained from this process was later used as substrate.

Synthesis of $Fe_5C_2@Ns$ -rGO/CNT nanocatalyst: The s-rGO (0.15g) was mixed with porphyrin (0.77g), and azodicarboxamide (1.62 g) in acetonitrile (20 mL) by stirring it for 30 min. Then, the well-dispersed mixture was irradiated by electromagnetic wave using household microwave oven (KR-H20MT, Daewoo electronics) at 700W for 300 sec. After microwave treatment, the powder was transferred to an alumina boat in a tube-type furnace and was slowly heated at a ramping rate of $2.7^\circ C \cdot min^{-1}$ up to $350^\circ C$ under a flow of CO ($200 mL \cdot min^{-1}$) and then held at the same temperature for 4 h. After thermal treatment, the resulting powder was cooled to room temperature, and then submerged in ethanol (30 mL) under continuously flowing N_2 in order to minimize surface oxidation of the active catalyst. The powder in ethanol was simply separated using a magnet and dried in a vacuum oven at $60^\circ C$.

Synthesis of $Fe_5C_2@s$ -rGO/CNT, $Fe_5C_2@s$ -rGO and $Fe_5C_2@N$ -CNT nanocatalyst: To prepare the effect of hierarchical structure and n-doping were also synthesized for comparison. $Fe_5C_2@s$ -rGO/CNT was made by mixing the s-rGO (0.15g), ferrocene (0.77g), and azodicarboxamide (1.62 g) in acetonitrile (20 mL). $Fe_5C_2@s$ -rGO was used s-rGO (0.15g) and ferrocene (0.77g) in acetonitrile (20 mL) without azodicarboxamide. $Fe_5C_2@N$ -CNT was mixed MW-CNT (0.15g), porphyrin (0.77g), and azodicarboxamide (1.62g) in acetonitrile (20 mL). All mixtures were stirred for 30 min and irradiated by electromagnetic wave using same microwave oven at 700W for 300 sec, respectively. After microwave treatment, the powder samples were transferred to an alumina boat in a tube-type furnace and was slowly heated at a ramping rate of $2.7^\circ C \cdot min^{-1}$ up to $350^\circ C$ under a flow of CO ($200 mL \cdot min^{-1}$) and then held at the same temperature for 4 h. After thermal treatment, the resulting powder was cooled to

room temperature, and then submerged in ethanol under N₂ in order to minimize surface oxidation of the active catalyst. The powder in ethanol was simply separated using a magnet and dried in a vacuum oven at 60 °C.

Preparation of Fe₅C₂/AC catalyst: Iron (III) nitrate nonahydrate (1.28 g) and activated carbon (1.0 g) were physically ground in a mortar for 10 min under ambient conditions. Next, the mixed powder was placed in a polypropylene bottle and aged at 50 °C for 24 h in a tumbling oven. After aging, the sample cooled to room temperature was transferred to an alumina boat in a tube-type furnace. The powder mixture was slowly heated at a ramping rate of 2.7 °C·min⁻¹ up to 350 °C under a flow of CO (200 mL·min⁻¹) and then held at the same temperature for 4 h. After thermal treatment, the resulting powder was cooled to room temperature, and then submerged in ethanol under N₂. The powder immersed in ethanol was recovered using a magnet and dried.

High-temperature Fischer-Tropsch synthesis: The Fischer-Tropsch reaction tests were conducted using a fixed-bed reactor of stainless steel. The catalysts (20 mg) were diluted with glass beads (4.2 g, 425–600 μm) and then charged into the fixed-bed reactor. The catalysts were slightly oxidized during the catalyst loading process, but were reactivated under a CO flow of 40 mL·min⁻¹ at 350 °C for 4 h. After the activation treatment, reaction was carried out at 340 °C and 15 bar using a synthesis gas (H₂/CO = 1.0, GHSV = 210 NL·g_{cat}⁻¹·h⁻¹). The composition of the outlet gases was analysed using an online gas chromatograph (Agilent, 3000A Micro-GC) equipped with a molecular sieve and plot Q columns. The gas flow rates were measured using a wet-gas flow meter (Shinagawa Corp.). The composition of the wax and liquid products was analysed by means of an offline GC (Agilent, 6890 N) with a simulated distillation method (ASTM D2887).

Characterization: The morphology of the materials was analyzed with a JSM7500F and HITACHI S-4300 field emission scanning electron microscopy (FE-SEM) and a JEM-2100F ultra-corrected-energy-filtered transmission electron microscopy (US-EF-TEM) and an EDAX energy-dispersive spectrometer (EDS). The crystal structures were characterized by using an X-ray diffraction (XRD) using a D8 advance powder diffraction ($\lambda = 1.5406 \text{ \AA}$). The element compositions of the samples were collected by X-ray photoelectron spectroscopy (XPS) characterization using an ESCALAB 250 XPS system equipped with an Al K α X-ray radiation (1486.6 eV) as the X-ray source. The structural properties of the material were analyzed by the SENTERRA dispersive Raman. N₂ adsorption-desorption isotherms were obtained by a Brunauer-Emmett-Teller (BET) apparatus. The specific surface areas of the materials were calculated from BET method and the pore size distributions were derived by the BJH mode.

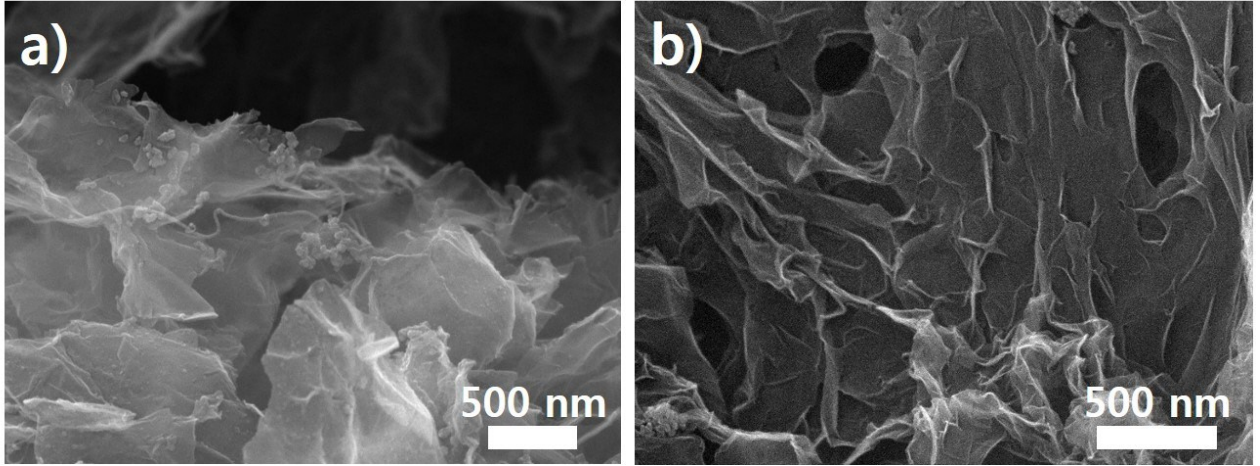


Figure S1. (a, b) SEM images of hybrid structure using rGO substrate.

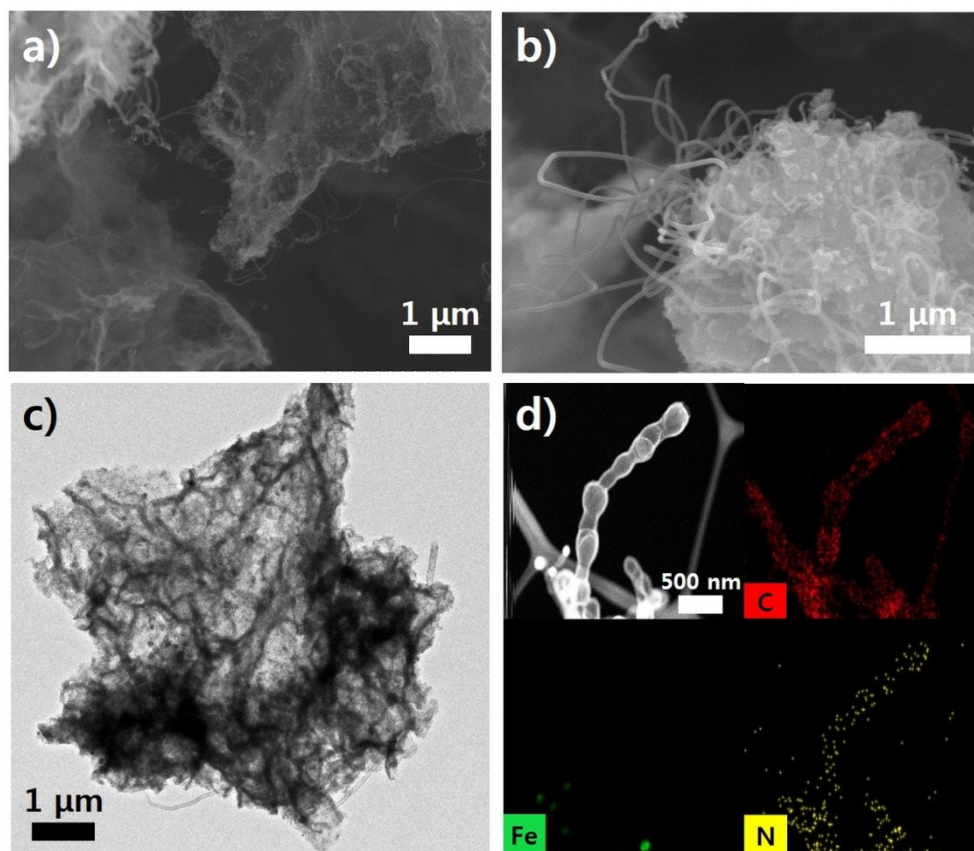


Figure S2. (a, b) SEM images, (c) TEM image, and (d) STEM images with elemental mappings of carbon, iron, and nitrogen of Fe@Ns-rGO/CNT.

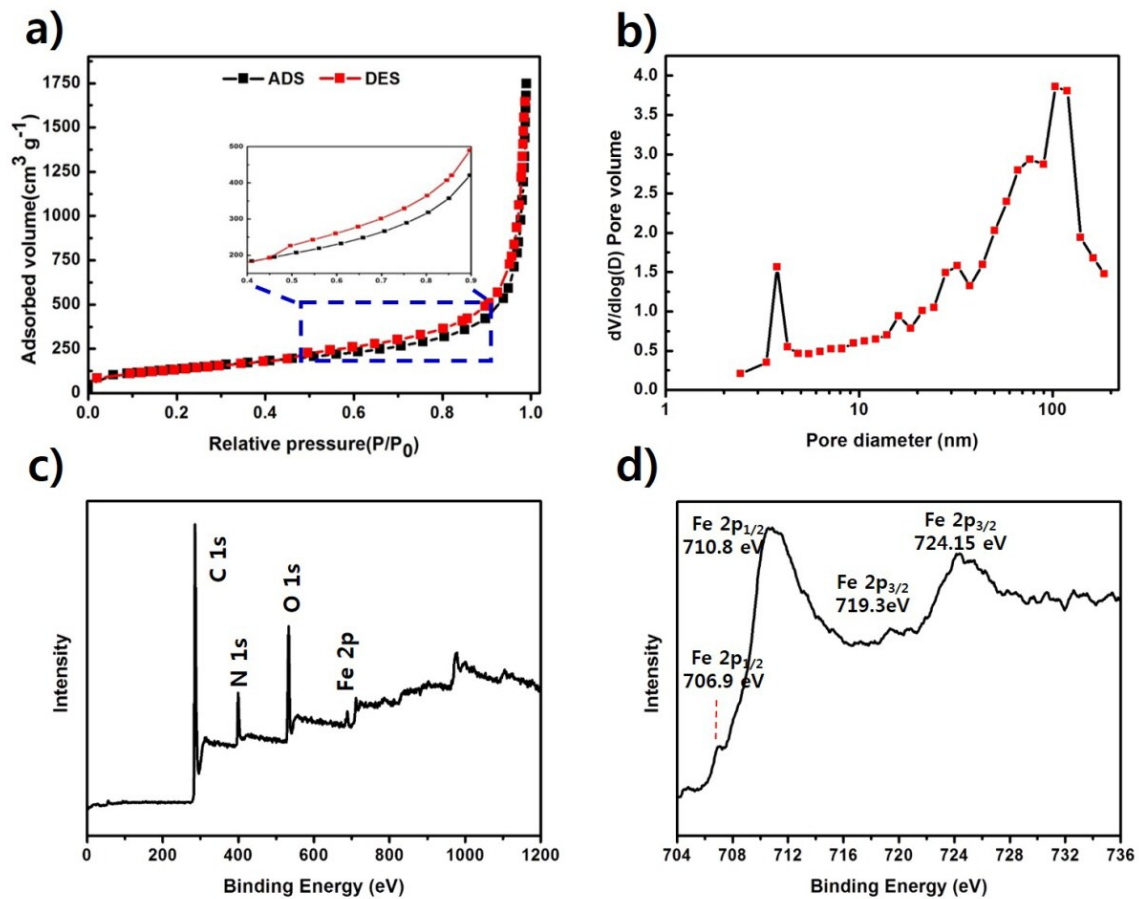


Figure S3. (a) N_2 adsorption/desorption isotherms, (b) Pore size distribution diagram calculated from desorption, (c) Survey XPS scan, (d) Fe 2p XPS scan of Fe@Ns-rGO/CNT.

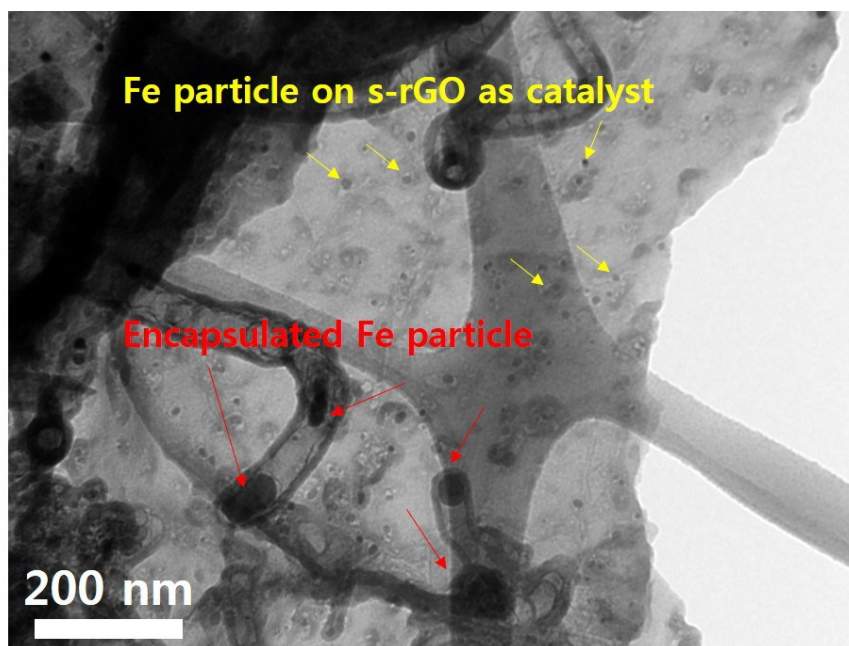


Figure S4. TEM image of the $\text{Fe}_5\text{C}_2@\text{Ns-rGO}/\text{CNT}$ nanocatalyst. Fe particles exposed on to the s-rGO surface (yellow) and encapsulated inside CNT (red).

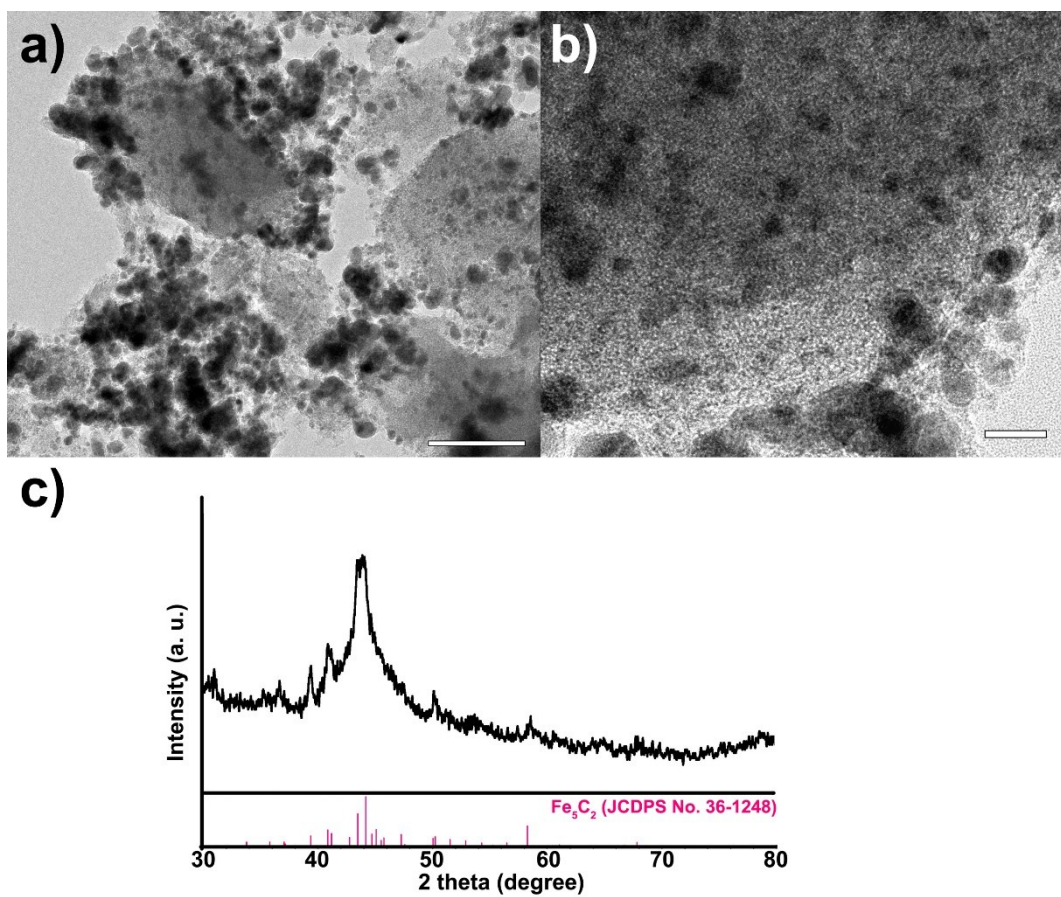


Figure S5. TEM images and XRD spectrum of Fe₅C₂/AC catalyst. The bars represent 200 nm (a) and 20 nm (b).

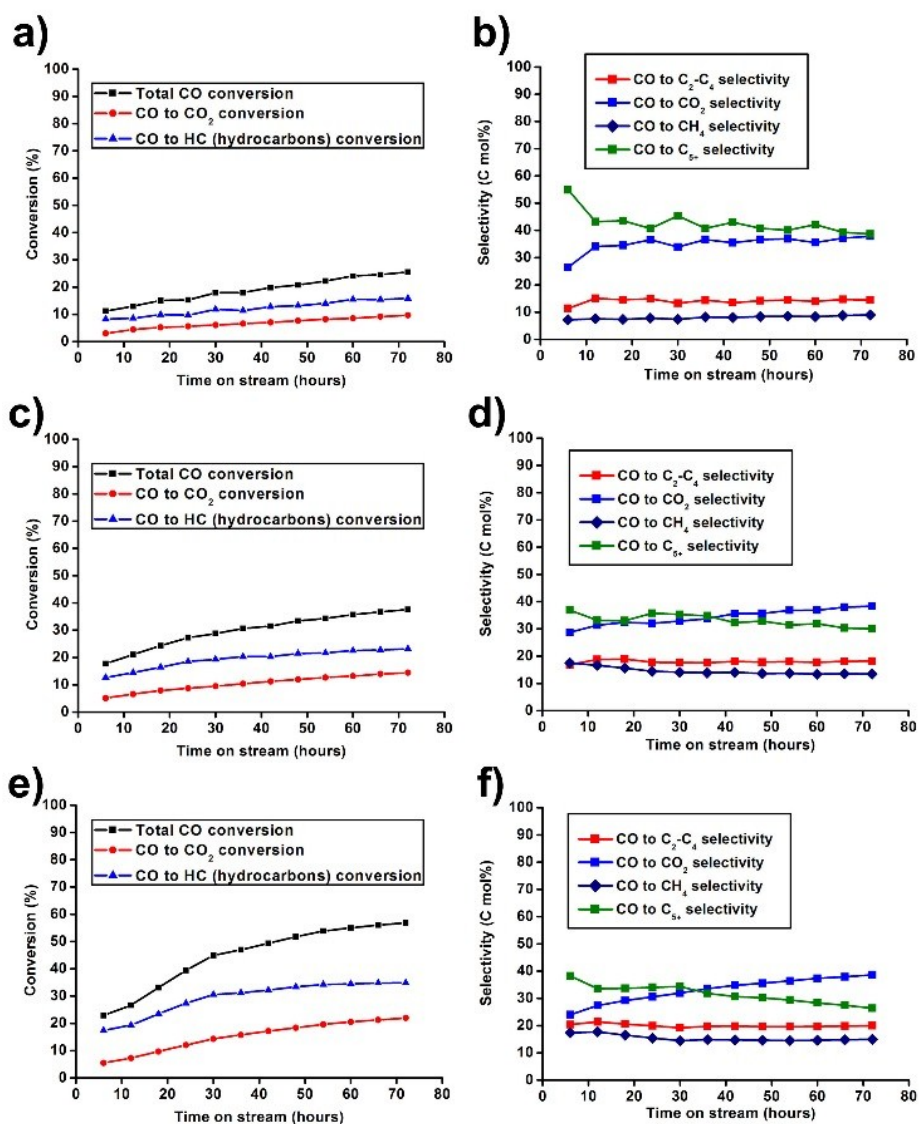


Figure S6. (a,c,e) CO conversion and (b,d,f) hydrocarbon product selectivity graphs. (a-b: Fe₅C₂@s-rGO/CNT, c-d: Fe₅C₂@N-CNT, e-f: Fe₅C₂@s-rGO). The reaction tests were conducted at 340 °C, 15 bar, GHSV 210 NL·g_{cat}⁻¹·h⁻¹ and H₂ : CO ratio of 1.

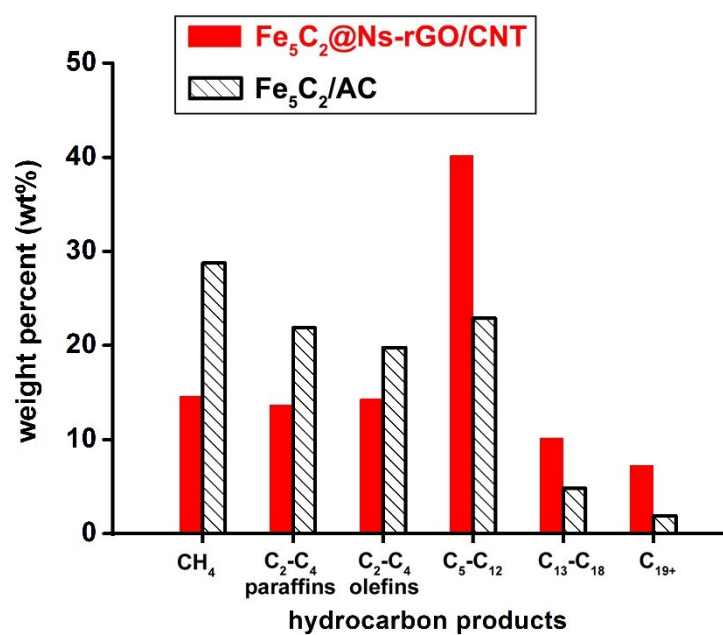


Figure S7. Hydrocarbon distribution of Fe₅C₂@Ns-rGO/CNT nanocatalyst and Fe₅C₂/AC catalysts for HT-FTS. The reaction tests were conducted at 340 °C, 15 bar, GHSV 210 NL·g_{cat}⁻¹·h⁻¹ and H₂ : CO ratio of 1.

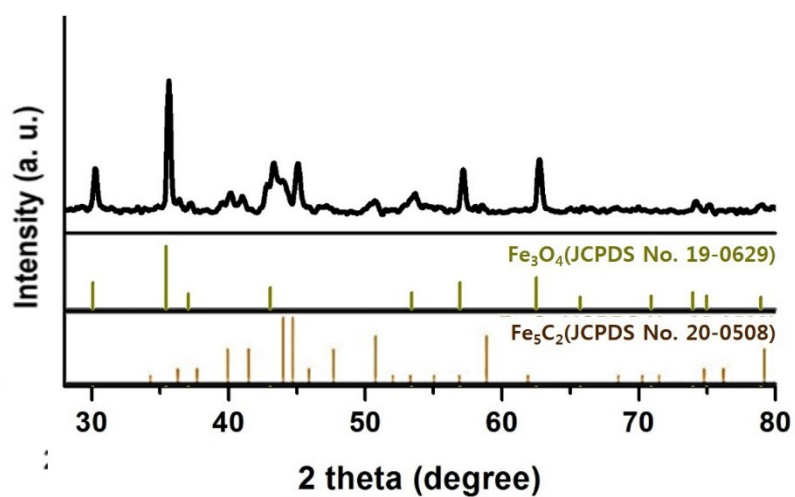


Figure S8. XRD spectrum of the recovered Fe₅C₂@Ns-rGO/CNT nanocatalyst after FTS for 72 h

Table S1. Comparison of the CO conversion and FTY values of the carbon-based Fe nanocatalysts for high-temperature Fischer-Tropsch synthesis reactions.

Catalyst	GHSV (NL·g _{cat} ⁻¹ ·h ⁻¹)	Total CO conv. (%)	FTY (×10 ⁻⁴ mol _{CO} ·g _{Fe} ⁻¹ ·s ⁻¹)	Ref.
Fe ₅ C ₂ @Ns-rGO/CNT (Fe: 14.5 wt%)	210	80	44.0	This work
Fe ₅ C ₂ /AC (Fe: 15 wt%)	210	40	22.3	This work
Fe ₅ C ₂ @CMK-3 (Fe: 20 wt%)	30	91.4	5.1	[1] ^a
Fe ₅ C ₂ @C catalyst diluted with activated charcoal (Fe: 20 wt%)	16	68	2.2	[2] ^a
	60.0	47	5.2	
K-doped Fe ₅ C ₂ /activated charcoal (Fe: 20wt%)	8	94	1.5	[3] ^a
Fe/CNT (Fe: 10 wt%)	16.2	85	4.7	[4] ^b
Fe@C (Fe: 25 wt%)	60	59	4.9	[5] ^c
FeK/rGO	72	58-64	6.5	[6] ^c
Fe/CNT (Fe: 10 wt%)	32	31.7	4.4	[7] ^d
Fe/CMK-3 (Fe: 10 wt%)		27.4	3.8	
Fe/activated carbon (Fe: 10 wt%)		37.6	5.2	
Fe ₂₀ K ₁₀ -graphene (Fe: 20 wt%)		2.5	81.5	
Fe@C-400 (Fe: 38 wt%)	30	74	3.8	[9] ^f
Fe/NCNT (Fe: 16 wt%)	50	56.5	7.8	[10] ^g
Fe-MIL-88B-NH ₂ /C (Fe: 32~34.1 wt%)	36	81.8	3.2	[11] ^h
	180	27.8	7.2	

Catalytic tests were carried out at ^aT = 320°C, P = 15 bar, H₂/CO ratio=1, ^bT = 300°C, P = 20 bar, H₂/CO ratio=2, ^cT = 340°C, P = 20 bar, H₂/CO ratio=1, ^dT = 300°C, P = 20 bar, H₂/CO ratio=2, ^eT = 325°C, P = 15 bar, H₂/CO ratio=2, ^fT = 340°C, P = 20 bar, H₂/CO ratio=1, ^gT = 340°C, P = 25 bar, H₂/CO ratio=1, ^hT = 300°C, P = 20 bar, H₂/CO ratio=1,

References

- [1] S. W. Kang, K. Kim, D. H. Chun, J.-I. Yang, H.-T. Lee, H. Jung, J. T. Lim, S. Jang, C. S. Kim, C.-W. Lee, S. H. Joo, J. W. Han, J. C. Park, *J. Catal.* **2017**, *349*, 66.
- [2] S. Y. Hong, D. H. Chun, J.-I. Yang, H. Jung, H.-T. Lee, S. Hong, S. Jang, J. T. Lim, C. S. Kim, J. C. Park, *Nanoscale* **2015**, *7*, 16616.
- [3] J. C. Park, S. C. Yeo, D. H. Chun, J. T. Lim, J.-I. Yang, H.-T. Lee, S. Hong, H. M. Lee, C. S. Kim, H. Jung, *J. Mater. Chem. A* **2014**, *2*, 14371.
- [4] V. V. Ordonsky, B. Legras, K. Cheng, S. Paul, A. Y. Khodakov, *Catal. Sci. Technol.* **2015**, *5*, 1433.

- [5] V. P. Santos, T. A. Wezendonk, J. J. D. Jaén, A. I. Dugulan, M. A. Nasalevich, H.-U. Islam, A. Chojecki, S. Sartipi, X. Sun, A. A. Hakeem, A. C. J. Koeken, M. Ruitenbeek, T. Davidian, G. R. Meima, G. Sankar, F. Kapteijn, M. Makkee, J. Gascon, *Nat. Commun.* **2015**, *6*, 6451.
- [6] Y. Cheng, J. Lin, K. Xu, H. Wang, X. Yao, Y. Pei, S. Yan, M. Qiao, B. Zong, *ACS Catal.* **2016**, *6*, 389.
- [7] K. Cheng, V. V. Ordonsky, M. Virginie, B. Legras, P. A. Chernavskii, V. O. Kazak, C. Cordier, S. Paul, Y. Wang, A. Y. Khodakov, *Appl. Catal. A* **2014**, *488*, 66.
- [8] S. O. Moussa, L. S. Panchakarla, M. Q. Ho, M. S. El-Shall, *ACS Catal.* **2014**, *4*, 535.
- [9] T. A. Wezendonk, V. P. Santos, M. A. Nasalevich, Q. S. E. Warringa, A. I. Dugulan, A. Chojecki, A. C. J. Koeken, M. Ruitenbeek, G. Meima, H.-U. Islam, G. Sankar, M. Makkee, F. Kapteijn, J. Gascon, *ACS Catal.* **2016**, *6*, 3236.
- [10] L. M. Chew, W. Xia, H. Düdder, P. Weide, H. Ruland, M. Muhler, *Catal. Today* **2016**, *270*, 85.
- [11] B. An, K. Cheng, C. Wang, Y. Wang, W. Lin, *ACS Catal.* **2016**, *6*, 3610.